Assessment of Physiological Distribution and Normal Variants of 68Ga PSMA-I&T PET/CT

Filiz Özülker [ID]

Department of Nuclear Medicine, Health Sciences University School of Medicine, Okmeydanı Health Application and Research Center, İstanbul, Turkey

Abstract

Objective: [68]Ga prostate-specific membrane antigen (PSMA) positron emission tomography/computerized tomography (PET/CT) imaging has been used efficiently in the evaluation of prostate cancer (PCa). There are three kinds of urea-based PSMA ligands labeled with ^{68}Ga, including PSMA 11, PSMA Imaging & Therapy (I&T), and PSMA 617. The aim of the present study was to investigate the *in vivo* distribution of the novel ligand PSMA I&T in normal tissues and to identify benign variants.

Methods: We retrospectively evaluated 34 patients with PCa who underwent ^{68}Ga PSMA I&T PET/CT imaging in our clinic between August 2017 and December 2017. Only patients who had no evidence of recurrent disease on conventional imaging performed before the ^{68}Ga PSMA I&T PET/CT scan were included in the study. Patients also had no ^{68}Ga PSMA avid lesion in favor of residual disease or recurrent disease on PET scan. The average age of the patients was 70.2±8.5 years.

Results: Evaluation of the conventional maximum intensity projection images revealed uptake of ^{68}Ga PSMA in the lacrimal, submandibular, and parotid glands; liver; spleen; kidneys; duodenum; jejunum; ileum; and urinary bladder. The radionuclide uptake of the body structures from the highest to the lowest in terms of SUVmax values was listed as kidneys, submandibular and parotid glands, urinary bladder, jejunum-ileum, lacrimal gland, duodenum, spleen, liver, and transverse colon. When SUVmean values are concerned, the list, from the highest to the lowest, was as follows: kidneys, urinary bladder, submandibular and parotid glands, duodenum, lacrimal gland, spleen, jejunum-ileum, liver, and transverse colon. We detected osteophytes in 15 patients, and 8 of them demonstrated mild uptake. We detected mild uptake in the celiac ganglia of 4 patients. We did not observe any physiological uptake in the surrenal glands, but there were two adenomas that show low degree of uptake. When double organs are compared, the SUVmax values of the right lacrimal, sublingual, and parotid glands were higher than those of the left counterparts, and differences were statistically significant (p<0.05), but there was not any statistically significant difference between the right and the left organs when SUVmean values were concerned. The liver showed less uptake, whereas blood pool showed more uptake when the distribution of PSMA I&T is compared with the studies made with the PSMA 11 ligand.

Conclusion: To our knowledge, this is the first study in the literature that aimed to reveal the distribution pattern of ^{68}Ga PSMA I&T. The *in vivo* distribution of PSMA I&T is almost congruent with the PSMA expression in the tissues defined with immunohistochemical results, and there are minor differences between PSMA 11 and PSMA I&T regarding normal tissue uptake.

Keywords: [68]Ga PSMA I&T, biodistribution, PET/CT, prostate cancer, prostate, prostate-specific membrane antigen

ORCID ID of the author:
F.Ö. 0000-0003-2075-1429

Corresponding Author:
Filiz Özülker

E-mail:
tozulker@gmail.com

INTRODUCTION

Prostate cancer (PCa) is the most frequently diagnosed tumor in men worldwide, and its incidence has been increasing in recent years (1). Conventional imaging methods, such as multiparametric magnetic resonance imaging (mpMRI) and choline positron emission tomography/computerized

tomography (PET/CT), have been used widely for the purpose of primary staging and detecting the locoregional recurrences. Recently, ^{68}Ga-labeled prostate-specific membrane antigen (PSMA) inhibitor, Glu-NH-CO-NH-Lys (Ahx)-HBED-CC (^{68}Ga PSMA 11), a urea-based PSMA inhibitor, was introduced as a promising PET tracer for the evaluation of PCa (2, 3). PSMA is a type II membrane protein with folate hydrolase activity produced by prostatic epithelium and is overexpressed on the surface of PCa cells (4). It is also expressed in extraprostatic tissues, including small bowel, salivary gland, and brain (4, 5). It is a cell surface protein with a transmembrane location and has an enzyme activity that enables the development of specific inhibitors and their internalization after binding of ligands (6). ^{68}Ga PSMA 11 binds efficiently to the transmembrane folate hydrolase receptor, which is also called as PSMA, and PET/CT imaging with this tracer has relatively high sensitivity in the detection of prostatic malignancies when compared with mpMRI and ^{18}F-choline PET/CT. There are also other urea-based PSMA ligands labeled with ^{68}Ga, including PSMA Imaging & Therapy (I&T) and PSMA 617 (7, 8). These PSMA ligands that use DOTAGA and DOTA conjugates enable binding with therapeutic radiometals rendering theranostic approach. Since PSMA is also expressed in several tissues other than benign prostate gland and prostate malignancies, the investigator should be familiar with the normal biodistribution of the radionuclide in order to avoid misinterpretation of the physiological uptake sites as malignant foci. Accumulation at the blood pool compartment in some visceral organs and uptake in some benign lesions and structures with unexplained mechanisms further complicate the interpretation of ^{68}Ga PSMA PET/CT studies.

Determining the uptake of ^{68}Ga PSMA in normal tissues is also important since the nature of the tumors is estimated by calculating the ratio between radiotracer uptake in tumor lesions and background. For this reason, there have been efforts to reveal the biodistribution map of ^{68}Ga PSMA (6, 9, 10). All of these studies used ^{68}Ga PSMA 11, which is the most commonly used ligand currently. At present, to our knowledge, there has been no study made for evaluating the physiological distribution of ^{68}Ga PSMA I&T. The aim of the present study was to investigate the uptake of this novel PSMA ligand in normal tissues and benign variants.

METHODS

Patients

We retrospectively evaluated 187 patients with PCa who underwent ^{68}Ga PSMA I&T PET/CT imaging in our clinic between August 2017 and December 2017 for the purpose of staging and restaging. The average age of the patients was 70.2±8.5 (65-82) years. Only patients who had no evidence of recurrent disease on conventional imaging performed before the ^{68}Ga PSMA I&T PET/CT scan were included in the present study. Patients also had no ^{68}Ga PSMA avid lesion in favor of residual disease or recurrent disease on PET scan. Therefore, 140 patients with metastatic disease were excluded from the study. Among 47 patients, 13, in whom there was extravasation of radionuclide, were excluded since it might yield false standardized uptake values (SUVs), and the remaining 34 were included in our study. Ethics committee approval was received for this study from the local ethics committee of Okmeydanı Research Hospital (Decision Date: 07/08/2018/Decision No: 961).

Radiolabeling

A fully automated Scintomics GRP synthesis module with Scintomics Control Center and GRP-Interface software was used for the radiolabeling of ^{68}Ga-DOTAGA-PSMA. The ^{68}Ge/^{68}Ga generator was purchased from iThemba LABS, South Africa. DOTAGA-PSMA was purchased from Scintomics GRP, Germany via a local distributor. The synthesis of the ^{68}Ga peptides was performed using a cationic purification method with 20 µg of peptide used for the reaction. The labeling efficiency and radiochemical purity were determined using radio thin-layer chromatography and radio-high-performance liquid chromatography. The radiochemical purities of ^{68}Ga-labeled PSMA conjugates were ≥95%.

Imaging

Patients were imaged using an integrated PET/CT scanner that consisted of a full-ring HI-REZ LSO PET and a six-slice CT scanner (Siemens Biograph 6, Chicago, IL, USA). Each patient was injected with a standardized weight-based dose of 2 MBq/kg (range 70-180 MBq), and images were obtained in a dual-phase mode. At 60 min post-injection, a whole-body PET/CT scan was conducted with an emission time of 3 min per bed position. Before emission images, a low-dose CT was performed for attenuation correction and anatomic localization with the following parameters: 50 mA, 140 kV, and 5 mm section thickness. All patients were positioned feet first, supine on the scanning pallet with imaging from the thigh to the vertex, and arms up.

Image Analysis

SUV_{max} and SUV_{mean} values were determined by a region of interest (ROI) applied in the transaxial attenuation-corrected PET slice with the highest uptake. ROIs obtained on CT images were applied to PET images for the following organs: bladder, nasal region, nasopharynx, aorta, left ventricle, stomach, duodenum, jejunum-ileum, rectum, cecum, transverse colon, spleen, and L5 vertebra. Symmetrical ROIs were obtained on both the left and right lacrimal glands, submandibular glands, parotid glands, nasolacrimal glands, vocal cords, lungs, kidneys, testes, femoral arteries, and gluteal muscles, and SUV_{max} and SUV_{mean} values were compared to determine if there was a difference between these double organs. The maximum SUV_{max} and SUV_{mean} values of the symmetrical organs are accepted as the representative value for that organ.

Statistical Analysis

The Statistical Package for Social Sciences version 22.0 (IBM SPSS Corp.; Armonk, NY, USA) program was used for statistical analysis. For data evaluation, the normal distribution fitness of the parameters was evaluated by the Shapiro-Wilk test. It was determined that the normal distribution was appropriate for the parameters. For comparison of descriptive statistical methods (mean and standard deviation) as well as quantitative data, the paired sample t-test was used for the right-left side comparisons of parameters. A p value <0.05 was considered as significant.

RESULTS

Evaluation of the conventional maximum intensity projection images revealed uptake of ^{68}Ga PSMA in the lacrimal, submandibular, and parotid glands; liver; spleen; kidneys; duodenum; jejunum; ileum; and urinary bladder (Figure 1). The radionuclide uptake of the body structures from the highest to the lowest in terms of SUV_{max} values were listed as kidneys, submandibular and parotid glands,
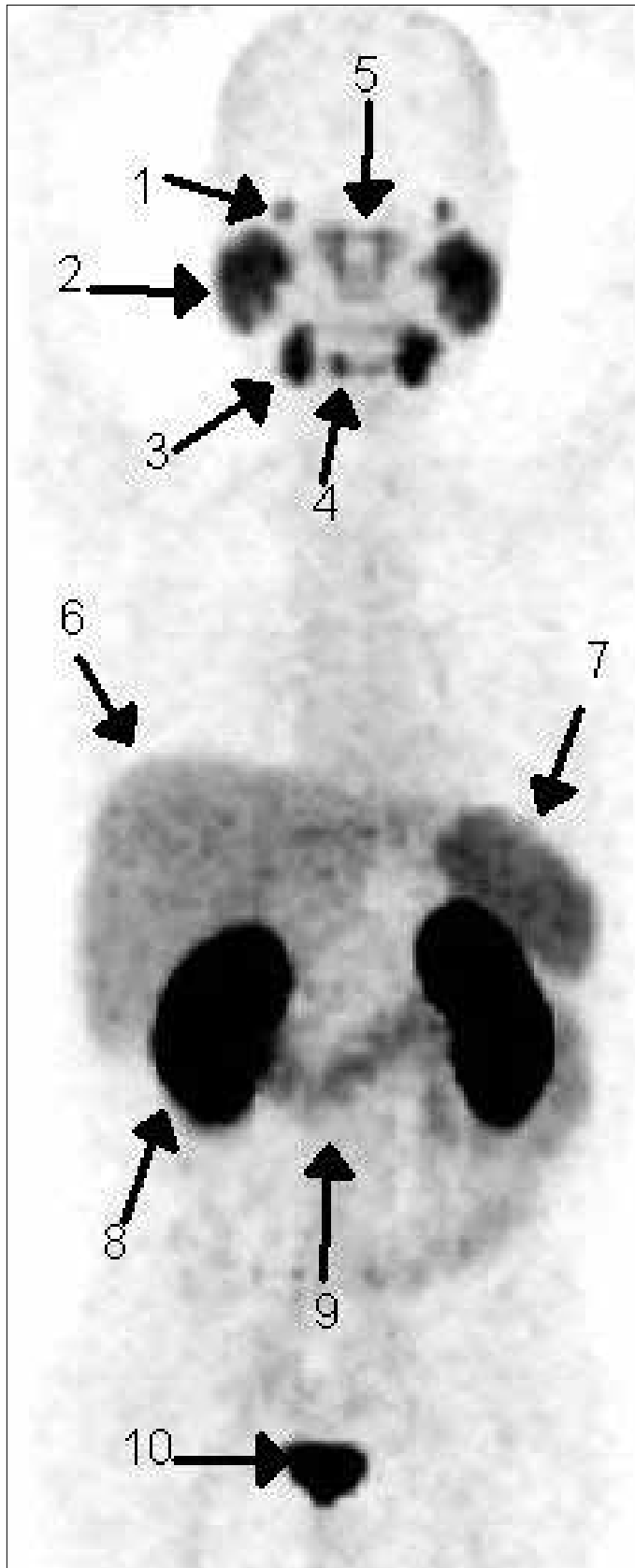
Figure 1. Normal ^{68}Ga PSMA uptake at the lacrimal glands (1), parotid glands (2), submandibular glands (3), sublingual glands (4), nasal region (5), liver (6), spleen (7), kidneys (8), small bowel (9), and urinary bladder (10)

urinary bladder, jejunum-ileum, lacrimal gland, duodenum, spleen, liver, and transverse colon. When SUV$_{mean}$ values are concerned, the list, from the highest to the lowest, was as follows: kidneys, urinary bladder, submandibular and parotid glands, duodenum, lacrimal gland, spleen, jejunum-ileum, liver, and transverse colon.

Table 1 shows the mean, standard deviation, and range of the measured SUVs for the organs and body structures showing ra-

Table 1. Minimum, maximum, mean and standard deviation values of SUV$_{max}$ and SUV$_{mean}$ values obtained from various organs of the patients

	SUV$_{max}$		SUV$_{mean}$	
	Range	Mean±SD	Range	Mean±SD
Right lacrimal gland	2.4-26.7	11.81±5.17	1.7-10	6.05±2.11
Left lacrimal gland	1.4-26.2	10.31±5	1-8.5	5.6±1.92
Right submandibular gland	10.7-38.6	21.21±6.25	4.7-20.9	11.52±3.28
Left submandibular gland	11.7-40.7	21.2±6.3	0.4-24.9	12.21±4.26
Right parotid gland	11.3-42	22.23±7.34	0.9-23.3	12.13±3.82
Left parotid gland	10-48.7	20.6±7.9	3.2-25.9	11.91±4.99
Nasal region	2.5-11.3	6.07±2.36	1.5-6	3.21±1.05
Right nasopharynx	3.3-12.2	6.64±2.43	2.4-8.5	4.63±1.66
Left nasopharynx	4.1-13.3	6.99±2.46	0.8-10.3	4.75±1.97
Vocal cord	2-11.2	5.01±1.89	1.5-6.5	3.05±1.09
Aort	1.1-5.8	3.37±0.92	0.4-3.5	1.87±0.63
Right lung	0.3-1.4	0.83±0.24	0.1-0.8	0.46±0.17
Left lung	0.2-1.8	0.9±0.34	0.1-1	0.49±0.2
Left ventricule	2.9-7.1	4.09±0.89	1.4-3.8	2.16±0.57
Stomach	1.6-7.2	3.84±1.47	0.9-4.8	2.26±0.96
Duodenum	4.4-21.8	10.98±4.13	2.7-16	6.24±2.98
Jejenum-ileum	6.3-22.2	13.03±4.35	2.4-10.5	4.59±1.8
Transverse colon	2.5-16.6	7.46±3.12	0.8-4.9	2.21±1.04
Cecum	1.7-5.3	3.11±0.88	0.5-3.4	1.63±0.57
Rectum	1.4-7.6	2.99±1.2	0.7-4.1	1.64±0.68
Liver	6.2-12.7	8.39±1.74	0.9-7.3	4.48±1.3
Spleen	5.1-27	9.59±4.35	1.1-19.7	5.96±3.39
Right kidney	22.4-89.3	59.86±15.53	13.5-44.8	29.64±6.99
Left kidney	23.5-98.7	59.61±16.2	1.1-43.3	28.43±8.67
Right femoral artery	0.8-4.3	2.37±0.74	0.5-2.1	1.18±0.35
Left femoral artery	1.3-5.2	2.35±0.76	0.4-2.2	1.2±0.38
Right testis	1.4-4.5	2.84±0.76	0.8-3.5	1.73±0.54
Left testis	1.5-4.6	2.99±0.84	0.5-3.2	1.75±0.55
Urinary bladder	4.7-51.4	18.51±11.1	2.7-88.7	14.98±15.13
Right gluteal muscle	0.7-2.8	1.24±0.41	0.3-1.5	0.65±0.23
Left gluteal muscle	0.8-3	1.41±0.49	0.1-1.3	0.73±0.28
L5 vertebra	1.6-4.7	2.72±0.76	0.6-2.2	1.29±0.39

dionuclide uptake. The mean, standard deviation, quartiles, and range of the maximum and mean SUVs of organs showing high and low radionuclide uptake are shown in Figure 2 and Figure 3, respectively.

The visual evaluation of the distribution of the radionuclide revealed the following observations from head to toe. The cerebral cortex did not show any uptake. There was not any uptake at hypophysis. Mild uptake was noted in the nasal region. The lacrimal, parotid, sublingual, and submandibular glands showed significant uptake bilaterally. There was mild symmetrical uptake at the vocal cords. The nasopharyngeal mucosa showed mild uptake of radionuclide. The thyroid gland had no uptake, and the thyroid nodule detected in a patient also did not show any uptake. The lung parenchyma did not exhibit considerable radionuclide uptake except a low-intensity uptake at an opacity representing the fibrotic scar tissue (SUV_{max} 1.7 and SUV_{mean} 1).

Meanwhile, the mediastinal lymph nodes did not show any uptake. We did not observe any physiological uptake in the surrenal glands, but there was a subcentimetric surrenal adenoma in a patient who showed mild radionuclide uptake (SUV_{max} 4.5 and SUV_{mean} 3), and in another patient, a surrenal adenoma with a diameter of 12 mm also showed similarly low degree of uptake (SUV_{max} 4.6 and SUV_{mean} 3.4). The liver had a diffuse and homogenous activity with average values of SUV_{max} 8.39±1.74 and SUV_{mean} 4.48±1.3. The activity uptake in the spleen was also homogenous but slightly higher than the uptake in the liver (mean values; SUV_{max} 9.59±4.35 and SUV_{mean} 5.96±3.39). The small intestines demonstrated significant uptake, most intense at the jejunum–ileum (SUV_{max} 13.03±4.35) and to a lesser extent at the duodenum (SUV_{max} 10.98±4.13). There was variable and mild uptake at the transverse colon, and no uptake was detected in other segments of the large intestine. The kidneys showed intense accumulation of radionuclide especially at the cortex. Although the radionuclide is excreted in urine, there was no significant uptake in the renal pelvis. In two patients, the ureters showed mild uptake, bilaterally in one patient and unilaterally in another. Meanwhile, there was significant accumulation of radionuclide in the
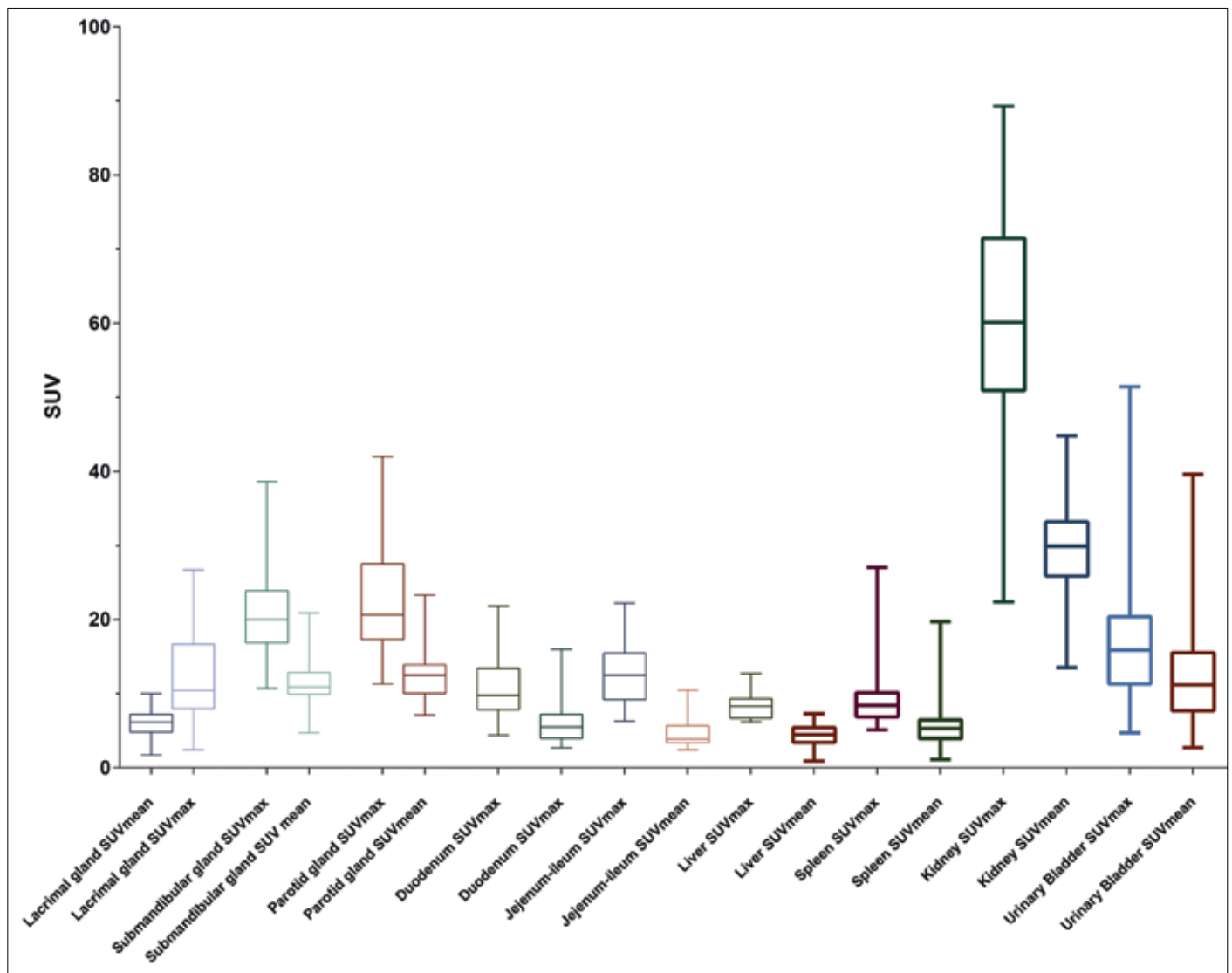

Figure 2. The mean, standard deviation, quartiles, and range of maximum and mean SUVs of organs showing high radionuclide uptake

urinary bladder. We detected mild uptake in the celiac ganglia of four patients. Mild physiological uptake was observed in the L5 vertebra on which the ROI was obtained (SUV_{max} 2.72±0.76), and similar activity was detected in the fracture sites at the two ribs of a patient (SUV_{max} 2.7 and SUV_{mean} 1.4). In our study group, we detected osteophytes in 15 patients, and 8 of them demonstrated mild uptake. The average SUV_{max} and SUV_{mean} values were 3.95±1.1 and 2.5±0.6, respectively. Out of 15 Schmorl nodules detected in these patients, only one of them showed uptake (SUV_{max} 4.3 and SUV_{mean} 1.5). The stomach showed mild uptake.

A normal gall bladder had no uptake, and an incidentally detected gall bladder stone on the CT part of the study also did not show any uptake.

When double organs are compared, the SUV_{max} values of the right lacrimal, parotid, sublingual, and parotid glands were higher than those of the left counterparts, and the differences were statistically significant (p<0.05), but there was not any statistically significant difference between the right and the left organs when SUV_{mean} values were concerned. The PET and CT images showing some of the physiological uptake sites and benign variants are displayed in Figure 4 and 5, respectively.

DISCUSSION

There have been studies to investigate the distribution pattern of ^{68}Ga PSMA 11, provide the average values of normal SUVs in various body structures, and compare the results with the *in vitro* expression of PSMA 11 (9, 11). No study has been made with the newly developed ligand PSMA I&T with the above-mentioned purposes. McCarthy et al. explored any possible difference regarding the diagnostic efficacy between PSMA I&T and PSMA-HBED and also made the comparison of biodistribution of these two ligands. According to their study, PSMA 11 demonstrated lower SUV_{mean} activity for blood pool and for bone, meanwhile the activity in the liver was greater than PSMA I&T. Their comparative study demonstrated higher lesional PSMA 11 binding than PSMA I&T (8). In the present study, the biodistribution of PSMA I&T was found to be almost similar to that of PSMA 11. PSMA is expressed not only in the prostate epithelium but also in the tissues, such as duodenal mucosa, a subset of renal tubules,
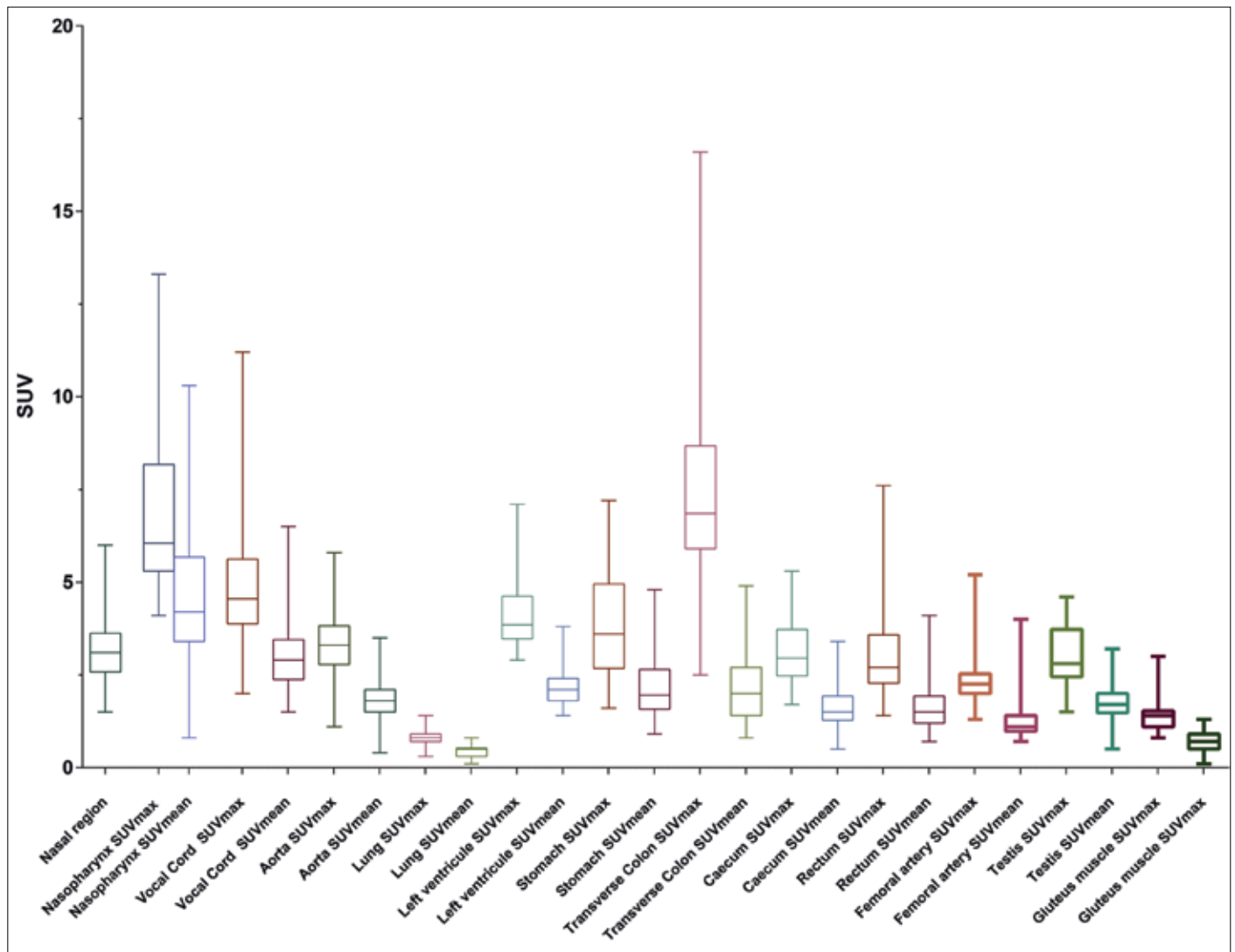

Figure 3. The mean, standard deviation, quartiles, and range of maximum and mean SUVs of organs showing low radionuclide uptake

and certain neuroendocrine cells in colonic crypts as well (5). It was also detected in the bladder, testis, ovary, fallopian tube, breast, adrenal gland, liver, esophagus, stomach, salivary gland, and brain with immunohistochemical staining (12).

In our study, the cerebral cortex did not show any uptake of PSMA I&T, as it was the case with PSMA 11. Demirci et al. (10) ex-
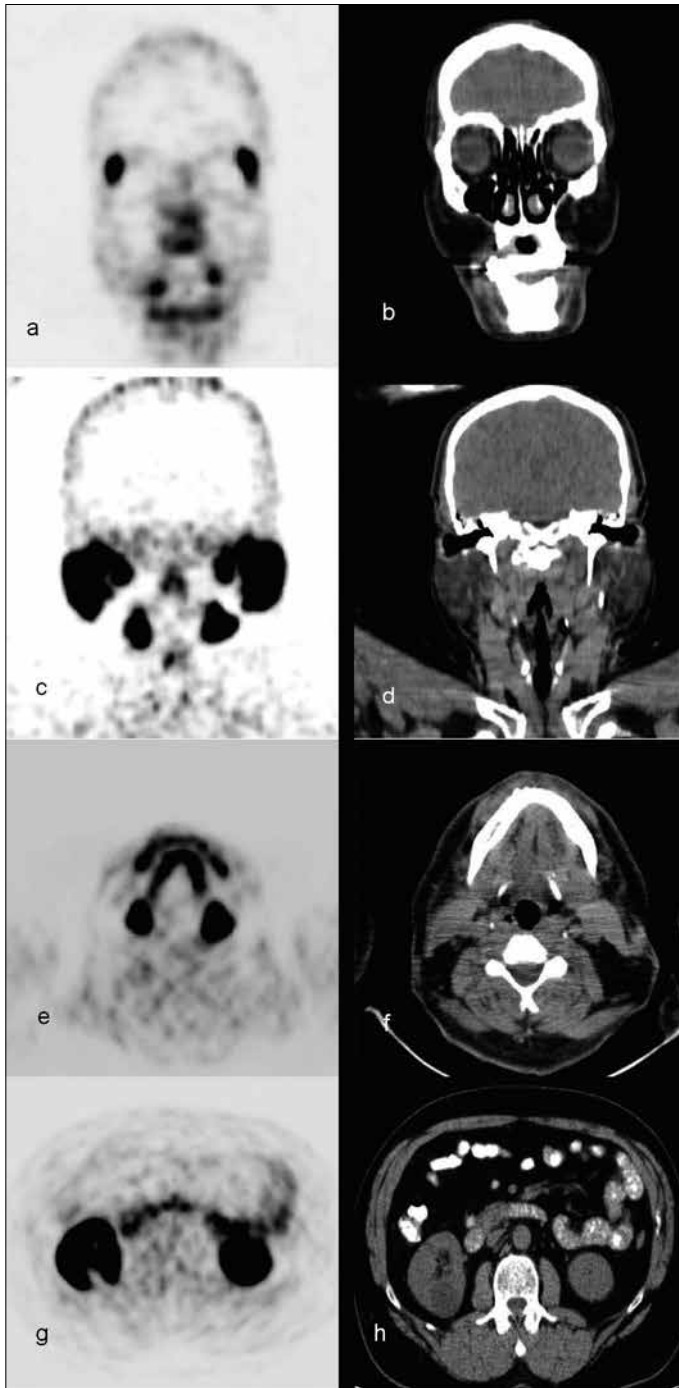
plained this fact with the inability of the tracer passing through the blood–brain barrier and the intracytoplasmic expression of the PSMA in the brain. Therefore, although immunohistochemical studies showed CNS staining in the hippocampal neurons and astrocytes, no ^{68}Ga PSMA activity is seen (12). Mild uptake was seen in the nasal region that is attributed to the PSMA expression in areas of tissue regeneration or a blood pool effect (6). In our series, nasopharyngeal uptake was localized mostly in the torus tubarius region as in the study by Nulent et al. (13). The parotid, submandibular, sublingual, and lacrimal glands showed diffuse and intense uptake. The salivary glands were the second highest activity-accumulating organ after the kidneys when SUV_{max} values are concerned. According to immunohistochemical staining results, PSMA in human salivary gland specimens is expressed on the epithelium of the acinar glandular cells and not the duct cells (14). Depending on its expression site, in a study, it is hypothesized that uptake of PSMA ligand is associated with gland volume and consequently shows the functional capacity of the gland (13). The average blood pool activity, measured from the ROIs obtained over the left ventricle, was found as SUV_{max} 4.09±0.89 and SUV_{mean} 2.16±0.57. McCarthy et al. (8) found statistically significant difference between average blood pool SUV_{mean} values of the two PSMA ligands, as PSMA 11 being 0.61±0.10 lower than I&T. Another study with PSMA 11 found the average SUV_{mean} for mediastinal blood pool as 1.5±0.5, which is also lower than our values (10). This relatively increased activity at blood pool might complicate the evaluation of the lesions where vascular structures are dominant. The liver and spleen demonstrated diffuse homogenously increased uptake with average values for the spleen (SUV_{max} 9.59±4.35 and SUV_{mean} 5.96±3.39) higher than the liver (SUV_{max} 8.39±1.74 and SUV_{mean} 4.48±1.3). Immunochemistry studies showed that the expression of PSMA in hepatocytes is weaker than that in the prostate and kidney (12). Additionally, the activity in the liver and spleen decreased in delayed images, as well as blood pool activity; thus, Afshar-Oromieh et al. (6) postulated that uptake in these tissues may be attributed to blood pool effect. The average SUV_{max} and SUV_{mean} values for the liver and spleen are found to be lower than those found by the study made with PSMA 11 (10). This finding is also in accordance with the comparison made by McCarthy et al. (8). According to immunohistochemical studies, whereas small bowel enterocytes showed strong staining, colon enterocytes exhibited weak to moderate staining for PSMA (12). Our findings for radionuclide uptake in the small and large bowel were concordant with this *in vitro* distribution pattern of PSMA, and the duodenum and jejunum–ileum showed significant uptake, whereas the transverse colon and cecum displayed minor uptake. Although normal transitional epithelium of the bladder was positively stained for PSMA (12), it showed unproportionally high radionuclide uptake that is mostly attributed to excretion of radionuclide in urine. There was no remarkable radionuclide uptake in the surrenal glands although immunohistochemistry detected weak to moderate amount of PSMA exhibition within the zona reticularis, cortex, and medulla (12). There have been reported cases of visualization of adenomas in the surrenal glands (10, 15), and we observed mild uptake at 2 out of 5 adrenal adenomas that were detected incidentally. The stomach showed mild uptake (SUV_{max} 3.84±1.47 and SUV_{mean} 2.26±0.96) despite the weak to

Figure 4. a-h. PET and CT images showing normal ^{68}Ga PSMA uptake at lacrimal glands (a, b), parotid and salivary glands (c, d), submandibular and sublingual glands (e, f), kidneys and small bowel (g, h)
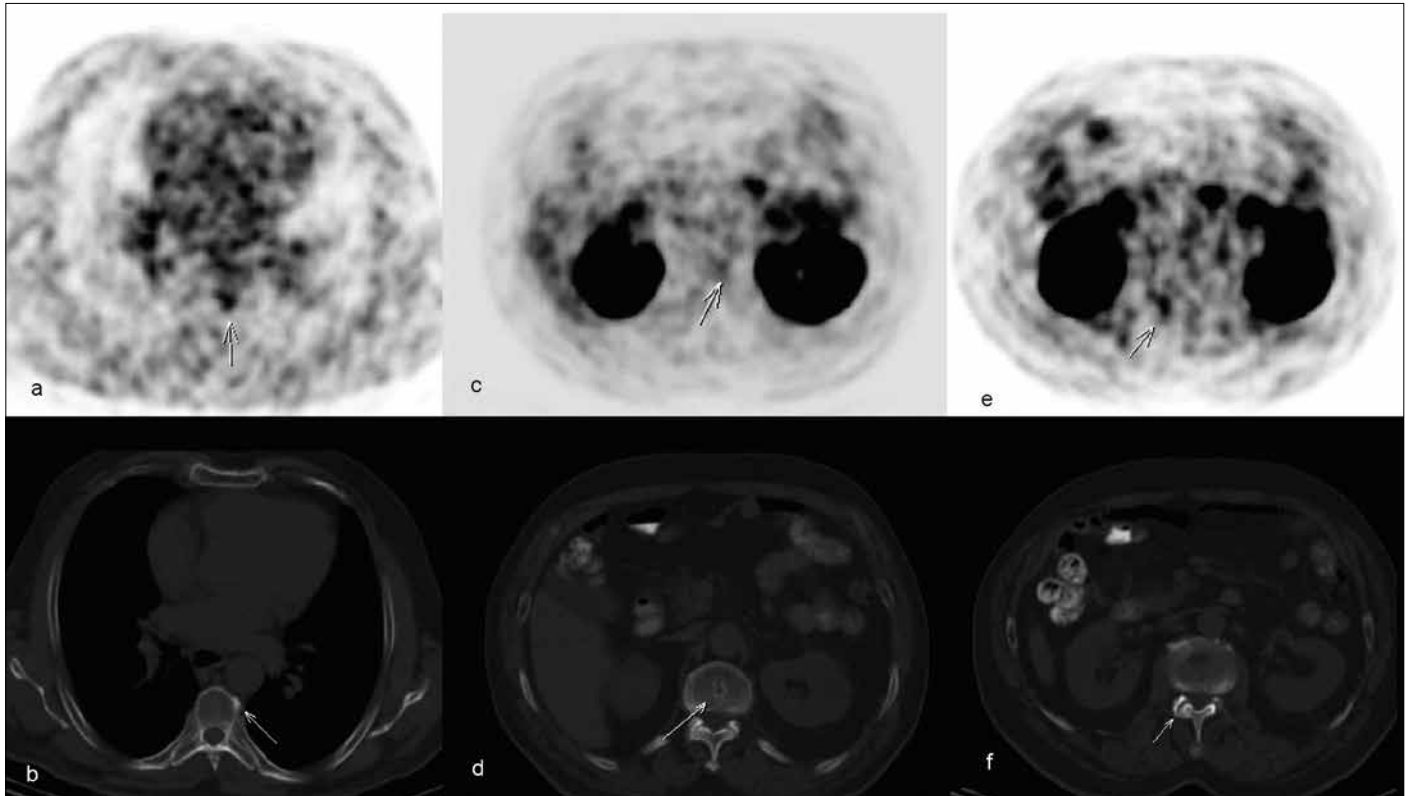PET: positron emission tomography; CT: computerized tomography

Figure 5. a-d. Axial PET and CT images displaying ⁶⁸Ga PSMA uptake at osteophyte (a, b), Schmorl nodule (c, d), and degenerative process
PET: positron emission tomography; CT: computerized tomography

negative staining for PSMA at the surface foveolar epithelia (12). We could not detect uptake at the gall bladder unlike the study by Demirci et al. (10) in which they reported gall bladder uptake in 10% of the patients. Physiological uptake in the celiac and stellate ganglia is a frequently encountered finding on ⁶⁸Ga PSMA 11 PET/CT imaging. Kanthan et al. reported that 94% of the patients demonstrate uptake in at least one of the four ganglia studied on PSMA-HBED PET/CT scan (16). In our study, we have only detected celiac ganglia in 4 (11.7%) patients. This low rate of detection can be explained with the effect of the algorithm used for reconstruction and resolution limitations of the PET/CT device rather than being a characteristic of the ⁶⁸Ga PSMA I&T (16).

⁶⁸Ga PSMA also shows uptake in benign and physiological variants necessitating to be familiar with while interpreting the images, otherwise it might cause misleading results. Osteophytes, Schmorl nodules, and rib fractures were among these lesions that we encountered in our study.

A limited number of studies that have been made to compare the efficacies of ⁶⁸Ga PSMA I&T with ⁶⁸Ga PSMA 11, in the detection rates for recurrent PCa, revealed comparable results (8, 17). These studies also aimed to evaluate the biodistribution of radiotracer and identification of normal SUVs for the body structures, but they had a main limitation of choosing the subjects from patients with metastases. Radionuclide uptake in the normal organs and tissues is dependent on tumor load, and high tumor burden might result in 58% and 64% decrease in the normal structures (18).

CONCLUSION

To the best of our knowledge, this is the first study in the literature that aimed to reveal the distribution pattern of ⁶⁸Ga PSMA I&T. We also mentioned the benign variants showing radiotracer uptake to avoid misleading results. Further studies to compare the biodistribution of different PSMA ligands among patients without metastatic tumor burden will be helpful to conduct more realistic *in vivo* mapping of ⁶⁸Ga PSMA.

REFERENCES

1. Pernar CH, Ebot EM, Wilson KM, Mucci LA. The Epidemiology of Prostate Cancer. Cold Spring Harb Perspect Med 2018 Jan 8. doi: 10.1101/cshperspect.a030361. [Epub ahead of print] [CrossRef]

2. Schäfer M, Bauder-Wüst U, Leotta K, Zoller F, Mier W, Haberkorn U et al. A dimerized urea-based inhibitor of the prostate-specific membrane antigen for 68Ga-PET imaging of prostate cancer. EJNMMI Res 2012; 2: 23. [CrossRef]

3. Eder M, Schäfer M, Bauder-Wüst U, Hull WE, Wängler C, Mier W et al. 68Ga-complex lipophilicity and the targeting property of a urea-based PSMA inhibitor for PET imaging. Bioconjug Chem 2012; 23: 688-97. [CrossRef]

4. Israeli RS, Powell CT, Corr JG, Fair WR, Heston WD. Expression of the prostate-specific membrane antigen. Cancer Res 1994; 54: 1807-11.

5. Silver DA, Pellicer I, Fair WR, Heston WD, Cordon-Cardo C. Prostate specific membrane antigen expression in normal and malignant human tissues. Clin Cancer Res 1997; 3: 81-5.

6. Afshar-Oromieh A, Malcher A, Eder M, Eisenhut M, Linhart HG, Hadaschik BA et al. PET imaging with a [68Ga]gallium-labelled PSMA ligand for the diagnosis of prostate cancer: biodistribution in humans and first evaluation of tumour lesions. Eur J Nucl Med Mol Imaging 2013; 40: 486-95. [CrossRef]

7. Ceci F, Castellucci P, Cerci JJ, Fanti S. New aspects of molecular imaging in prostate cancer. Methods 2017; 130: 36-41. [CrossRef]

8. McCarthy M, Langton T, Kumar D, Campbell A. Comparison of PSMA-HBED and PSMA-I&T as diagnostic agents in prostate carcinoma. Eur J Nucl Med Mol Imaging 2017; 44: 1455-62. [CrossRef]

9. Prasad V, Steffen IG, Diederichs G Makowski MR, Wust P, Brenner W. Biodistribution of [68Ga]PSMA-HBED-CC in Patients with Prostate Cancer: Characterization of Uptake in Normal Organs and Tumour Lesions. Mol Imaging Biol 2016; 18: 428-36. [CrossRef]

10. Demirci E, Sahin OE, Ocak M, Akovali B, Nematyazar J, Kabasakal L. Normal distribution pattern and physiological variants of 68Ga-PSMA-11 PET/CT imaging. Nucl Med Commun 2016; 37: 1169-79. [CrossRef]

11. Komek H, Morcali H, Altindag S, Can C, Uğur T. Biodistribution of Ga 68 Psma in Normal Organs J hum rhythm 2017; 3: 50-5.

12. Kinoshita Y, Kuratsukuri K, Landas S, Imaida K, Rovito PM Jr, Wang CY et al. Expression of prostate-specific membrane antigen in normal and malignant human tissues. World J Surg 2006; 30: 628-36. [CrossRef]

13. Klein Nulent TJW, Valstar MH, de Keizer B, Willems SM, Smit LA, Al-Mamgani A, et al. Physiologic distribution of PSMA-ligand in salivary glands and seromucous glands of the head and neck on PET/CT. Oral Surg Oral Med Oral Pathol Oral Radiol 2018; 125: 478-86. [CrossRef]

14. Wolf P, Freudenberg N, Bühler P, Alt K, Schultze-Seemann W, Wetterauer U, et al. Three conformational antibodies specific for different PSMA epitopes are promising diagnostic and therapeutic tools for prostate cancer. Prostate 2010; 70: 562-9.

15. Law WP, Fiumara F, Fong W, Miles KA. Gallium-68 PSMA uptake in adrenal adenoma. J Med Imaging Radiat Oncol 2016; 60: 514-7. [CrossRef]

16. Kanthan GL, Hsiao E, Vu D, Schembri GP. Uptake in sympathetic ganglia on 68 Ga-PSMA-HBED PET/CT: A potential pitfall in scan interpretation. J Med Imaging Radiat Oncol 2017; 61: 732-8. [CrossRef]

17. Berliner C, Tienken M, Frenzel T, Kobayashi Y, Helberg A, Kirchner et al. Detection rate of PET/CT in patients with biochemical relapse of prostate cancer using [68Ga]PSMA I&T and comparison with published data of [68Ga]PSMA HBED-CC. Eur J Nucl Med Mol Imaging 2017; 44: 670-7. [CrossRef]

18. Gaertner FC, Halabi K, Ahmadzadehfar H, Kürpig S, Eppard E, Kotsikopoulos C, et al. Uptake of PSMA-ligands in normal tissues is dependent on tumor load in patients with prostate cancer. Oncotarget 2017; 8: 55094-103. [CrossRef]